

# Nucleon spin structure and pQCD frontier on the move

Roman S. Pasechnik\*

*High Energy Physics, Department of Physics and Astronomy,  
Uppsala University Box 516, SE-75120 Uppsala, Sweden*

Dmitry V. Shirkov and Oleg V. Teryaev

*Bogoliubov Lab, JINR, Dubna 141980, Russia*

Olga P. Solovtsova and Vyacheslav L. Khandramai

*Gomel State Technical University, Gomel 246746, Belarus*

(Dated: June 23, 2018)

## Abstract

The interplay between higher orders of the perturbative QCD (pQCD) expansion and higher-twist contributions in the analysis of recent Jefferson Lab data on the lowest moment of the spin-dependent proton  $\Gamma_1^p(Q^2)$  at  $0.05 < Q^2 < 3 \text{ GeV}^2$  is studied. We demonstrate that the values of the higher-twist coefficients  $\mu_{2k}^{p,n}$  extracted from the data by using the singularity-free analytic perturbation theory provide a better convergence of the higher-twist series than with the standard perturbative QCD. From the high-precision proton data, we extract the value of the singlet axial charge  $a_0(1 \text{ GeV}^2) = 0.33 \pm 0.05$ . We observe a slow  $Q^2$  dependence of fitted values of the twist coefficient  $\mu_4$  and  $a_0$  when going to lower energy scales, which can be explained by the renormalization group evolution of  $\mu_4(Q^2)$  and  $a_0(Q^2)$ . As the main result, a good quantitative description of all the Jefferson Lab data sets down to  $Q \simeq 350 \text{ MeV}$  is achieved.

PACS numbers: 11.10.Hi, 11.55.Hx, 11.55.Fv, 12.38.Bx, 12.38.Cy

---

\*Electronic address: roman.pasechnik@fysast.uu.se

## I. INTRODUCTION

The spin structure of the nucleon remains the essential problem of nonperturbative QCD and hadronic physics. One of its most significant manifestations is the so-called spin crisis or spin puzzle related to the surprisingly small fraction of proton polarization carried by quarks [1, 2]. This problem attracted attention to the peculiarities of the underlying QCD description of the nucleon spin, in particular, to the role of the gluonic anomaly (see [1, 3] and references therein). The natural physical interpretation of these effects was the gluon (circular) polarization, while the experimental indications of its smallness may also point to a possible manifestation of the anomaly via the strangeness polarization [4]. The key point is its consideration as a kind of heavy-quarks polarization [5] due to the multiscale [4] picture of the nucleon exploring the fact that strange quark mass is much (as the squared ratios matter) smaller than the nucleon one and, in turn, larger than higher-twist parameters.

Higher-twist parameters (known also as the color polarizabilities) are important ingredients of the nucleon spin structure. Their extraction from experimental studies is relatively complicated as they are most pronounced at low momentum transfer  $Q$ . Although in this region very accurate Jefferson Lab (JLab) data are now available, higher-twist contributions are shadowed by Landau singularities of QCD coupling. As was shown in Ref. [6], this problem may be solved by the use of singularity-free couplings which allowed a quite accurate extraction of higher twist (HT) and a fairly good description of data down to rather low  $Q$ . The object of investigation in [6] was the difference of the lowest moments  $\Gamma_1^{p,n}$  of proton and neutron structure functions  $g_1$ , which corresponds to the renowned Bjorken sum rule (BSR) [7]. At finite  $Q^2$  the moments  $\Gamma_1^{p,n}$  are modified by higher order radiative corrections and higher-twist power corrections, as dictated by the operator product expansion (OPE). Such generalized ( $Q^2$ -dependent) BSR became a convenient and renowned target ground for testing different possibilities of combining both the perturbative and nonperturbative QCD contributions in the low-energy domain (see, for example, Refs. [8, 9]).

The global higher twist analysis of the data on the spin-dependent proton structure function  $g_1^p$  at relatively large  $1 < Q^2 < 30 \text{ GeV}^2$ , was performed in Ref. [10]. While the  $1/Q^2$  term in the OPE works at relatively high scales  $Q^2 \gtrsim 1 \text{ GeV}^2$ , higher-twist power corrections  $1/Q^4$ ,  $1/Q^6$ , etc., start to play a significant role at lower scales, where the influence of the ghost singularities in the coefficient functions within the standard perturbation theory (PT) becomes more noticeable. It affects the results of extraction of the higher twists from the precise experimental data leading to unstable OPE series and huge error bars [6]. It seems natural that the weakening or elimination of the unphysical singularities of the QCD coupling would allow shifting the perturbative QCD (pQCD) frontier to a lower energy scale and getting more exact information about the nonperturbative part of the process described by the higher-twist series.

As was shown in Ref. [6], the situation becomes better if one uses for a running coupling a more precise iterative solution of the renormalisation group (RG) equation in the form of the so-called denominator representation [12] instead of the Particle Data Group loop  $1/L$  expansion [13], especially at the two-loop level. In this investigation, to avoid completely the unphysical singularities at  $Q = \Lambda_{QCD} \sim 400 \text{ MeV}$  we deal with the ghost-free analytic perturbation theory (APT) [14] (for a review on APT concepts and algorithms, see also Ref. [15]), which recently proved to be an intriguing candidate for a quantitative description of light quarkonia spectra within the Bethe-Salpeter approach [16], and the so-called glueball-freezing model proposed recently by Yu. A. Simonov in Ref. [17] (below, SGF model) to avoid

the renormalon [18] ambiguity in QCD. Other versions of frozen  $\alpha_s$  models were developed earlier in Ref. [19]. As it will be seen below that APT and SGF approaches predict very close couplings at  $Q \gtrsim \Lambda_{QCD}$ , whereas they have different infrared-stable points at  $Q = 0$ . Consequently, as it was shown in Ref. [6], these models lead to very close perturbative parts of the Bjorken sum  $\Gamma_{1,pert}^{p-n}$ . The higher-twist contributions turned out to be very close, too. Here, we would like to discuss this point in more detail.

In the current paper we study the interplay between higher orders of the pQCD expansion and higher-twist contributions using the recent JLab data on the lowest moments of the spin-dependent proton and neutron structure functions  $\Gamma_1^{p,n}(Q^2)$  and  $\Gamma_1^{p-n}(Q^2)$  in the range  $0.05 < Q^2 < 3 \text{ GeV}^2$  [11]. Thus, we extend and generalize the analysis started in Ref. [6] by considering also the singlet channel involving the  $\Gamma_1^{p,n}(Q^2)$  for the proton (providing the most accurate data) and the neutron structure functions separately. This allows, in particular, determining the singlet axial charge  $a_0$  coming into both  $\Gamma_1^{p,n}(Q^2)$  moments, which in the quark-parton model is identified with the total spin carried by quarks in the proton. For this purpose, we perform the global analysis of the JLab precise low-energy data on  $\Gamma_1^p(Q^2)$  [20] using the advantages of the APT and SGF model, and extract the singlet axial charge  $a_0$ , as well as the coefficient  $\mu_4^{p,n}$  of the  $1/Q^2$  subleading twist-4 term, which contains information on quark-gluon correlations in nucleons.

The paper is organized as follows. In Sec. 2, the lowest moments analysis for the polarized structure functions  $g_1^{p,n}$  in the framework of the conventional PT approach is performed. In Sec. 3, we dwell briefly on the APT, its ideas and the results of its application to  $\Gamma_1^{p,n}(Q^2)$ . In Sec. 4, we apply the formalism to the analysis of the low-energy data on the first moments  $\Gamma_1^{p,n}(Q^2)$  and compare the results with the results of other researchers concerning the singlet axial constant  $a_0$  and gluon polarization  $\Delta g$  at low  $Q^2 \lesssim 1 \text{ GeV}^2$ . Section 5 contains discussion and some concluding remarks.

## II. SPIN SUM RULES IN CONVENTIONAL PT

### A. First moments of spin structure functions $g_1^{p,n}$

The lowest moments of spin-dependent proton and neutron structure functions  $g_1^{p,n}$  are defined as follows:

$$\Gamma_1^{p,n}(Q^2) = \int_0^1 dx g_1^{p,n}(x, Q^2), \quad (2.1)$$

with  $x = Q^2/2M\nu$ , the energy transfer  $\nu$ , and the nucleon mass  $M$ . The upper limit includes the proton/neutron elastic contribution at  $x = 1$ . This contribution becomes essential if the OPE is used to study the evolution of the integral in the moderate and low momentum transfer region  $Q^2 \lesssim 1 \text{ GeV}^2$  [21]. It is of special interest to analyze data with the elastic contribution excluded, since the low- $Q^2$  behavior of “inelastic” contributions to their nonsinglet combination  $\Gamma_1^{p-n}(Q^2)$ , i.e. BSR, is constrained by the Gerasimov-Drell-Hearn (GDH) sum rule [22], and one may investigate its continuation to a low scale [9]. So below we study inelastic contributions  $\Gamma_{inel,1}^{p,n}(Q^2)$  using the corresponding low-energy JLab data [20]. Note that the influence of the “elastic” contribution is noticeable starting from the higher-twist  $\sim \mu_6$  term which is natural due to a decrease of the elastic contribution with growing  $Q^2$  [6].

At large  $Q^2$  the moments  $\Gamma_1^{p,n}(Q^2)$  are given by the OPE series in powers of  $1/Q^2$  with the expansion coefficients related to nucleon matrix elements of operators of a definite twist

(defined as the dimension minus the spin of the operator), and coefficient functions in the form of pQCD series in  $\alpha_s^n$  (see, e.g., Ref. [23]). In the limit  $Q^2 \gg M^2$  the moments are dominated by the leading twist contribution,  $\mu_2^{p,n}(Q^2)$ , which is given in terms of matrix elements of the twist-2 axial vector current,  $\bar{\psi}\gamma^\mu\gamma_5\psi$ . This can be decomposed into flavor singlet and nonsinglet contributions. The total expression for the perturbative part of  $\Gamma_1^{p,n}(Q^2)$  including the HT contributions reads

$$\Gamma_1^{p,n}(Q^2) = \frac{1}{12} \left[ \left( \pm a_3 + \frac{1}{3} a_8 \right) E_{NS}(Q^2) + \frac{4}{3} a_0^{inv} E_S(Q^2) \right] + \sum_{i=2}^{\infty} \frac{\mu_{2i}^{p,n}(Q^2)}{Q^{2i-2}}, \quad (2.2)$$

where  $E_S$  and  $E_{NS}$  are the singlet and nonsinglet Wilson coefficients, respectively, calculated as series in powers of  $\alpha_s$  [24]. These coefficient functions for  $n_f = 3$  active flavors in the  $\overline{\text{MS}}$  scheme are

$$E_{NS}(Q^2) = 1 - \frac{\alpha_s}{\pi} - 3.558 \left( \frac{\alpha_s}{\pi} \right)^2 - 20.215 \left( \frac{\alpha_s}{\pi} \right)^3 - O(\alpha_s^4), \quad (2.3)$$

$$E_S(Q^2) = 1 - \frac{\alpha_s}{\pi} - 1.096 \left( \frac{\alpha_s}{\pi} \right)^2 - O(\alpha_s^3). \quad (2.4)$$

The triplet and octet axial charges  $a_3 \equiv g_A = 1.267 \pm 0.004$  [13] and  $a_8 = 0.585 \pm 0.025$  [25], respectively, are extracted from weak decay matrix elements and are known from  $\beta$ -decay measurements. As for the singlet axial charge  $a_0$ , it is convenient to work with its RG invariant definition in the  $\overline{\text{MS}}$  scheme  $a_0^{inv} = a_0(Q^2 = \infty)$ , in which all the  $Q^2$  dependence is factorized into the definition of the Wilson coefficient  $E_S(Q^2)$ .

In contrast to the proton and neutron spin sum rules (SSRs), the singlet and octet contributions are canceled out, giving rise to more fundamental BSR

$$\Gamma_1^{p-n}(Q^2) = \frac{g_A}{6} E_{NS}(Q^2) + \sum_{i=2}^{\infty} \frac{\mu_{2i}^{p-n}(Q^2)}{Q^{2i-2}}, \quad (2.5)$$

which is analyzed here along with the proton SSR in more detail than in Ref. [6]. The first nonleading twist term [26] can be expressed [27]

$$\mu_4^{p-n} \approx \frac{4M^2}{9} f_2^{p-n},$$

in terms of the color polarizability  $f_2$ .

The RG  $Q^2$  evolution of the axial singlet charge  $a_0(Q^2)$  and nonsinglet higher-twist  $\mu_4^{p-n}(Q^2)$  is [26]

$$a_0(Q^2) = a_0(Q_0^2) \exp \left\{ \frac{\gamma_2}{(4\pi)^2 \beta_0} [\alpha_s(Q^2) - \alpha_s(Q_0^2)] \right\}, \quad \gamma_2 = 16n_f, \quad (2.6)$$

$$\mu_4^{p-n}(Q^2) = \mu_4^{p-n}(Q_0^2) \left[ \frac{\alpha_s(Q^2)}{\alpha_s(Q_0^2)} \right]^{\gamma_0/8\pi\beta_0}, \quad \beta_0 = \frac{33 - 2n_f}{12\pi}, \quad \gamma_0 = \frac{16}{3} C_F. \quad (2.7)$$

In the NLO we may write

$$a_0(Q^2) \simeq a_0(Q_0^2) [1 + \Delta_1(Q^2) + \mathcal{O}(\alpha_s^2)], \quad (2.8)$$

$$\Delta_1(Q^2) = \frac{\gamma_2}{(4\pi)^2 \beta_0} [\alpha_s(Q^2) - \alpha_s(Q_0^2)], \quad \frac{\gamma_2}{(4\pi)^2 \beta_0} = \frac{4}{3\pi}.$$

As a first step of our analysis, in Eq. (2.2) we will neglect the weak dependence of  $\mu_{2i}^{p,n}$  on  $\log Q^2$ . Note that the evolution of the higher-twist terms  $\mu_{6,8,\dots}$  in Eq. (2.2) is still unknown. As a next step we discuss the possible influence of the  $\mu_4(Q^2)$  evolution on our results. The  $Q^2$  evolution of the proton higher-twist term  $\mu_4^p(Q^2)$  is assumed to be the same as the evolution of the nonsinglet twist  $\mu_4^{p-n}(Q^2)$ . This may be justified by the relative smallness of the singlet higher-twist term.

TABLE I: Current NLO fit results for the axial singlet charge  $a_0$ .

Reference	LSS [30]	DSSV [31]	AAC [32]	HERMES [29]	COMPASS [28]
$Q_0^2$ , GeV <sup>2</sup>	1.0	10.0	4.0	5.0	3.0
$a_0$	$0.24 \pm 0.07$	0.24	$0.25 \pm 0.05$	$0.32 \pm 0.04$	$0.35 \pm 0.06$

Let us discuss current results for the nucleon spin structure and higher twists. In Table I, we list the fit results for the axial singlet charge  $a_0$  from the literature including all global NLO PT analyses and the recent results obtained directly from deuteron data on  $\Gamma_1^d$  by COMPASS [28] and HERMES [29]. The global fit results for  $a_0$  are somewhat lower than that from the deuteron data. It was mentioned in the most recent review [2] that the reason for such a discrepancy is not completely understood. Further, we analyze this issue in more detail.

TABLE II: Current NLO fit results for the highest-twist term  $\mu_4/M^2$ . The uncertainties are statistical only.

Target	Proton [36]	Neutron [37]	p - n [38]	p - n [35]	p - n [6]
$Q^2$ , GeV <sup>2</sup>	0.6 - 10.0	0.5 - 10.0	0.5 - 10.0	0.66 - 10.0	0.12 - 3.0
$\mu_4/M^2$	$-0.065 \pm 0.012$	$0.019 \pm 0.002$	$-0.06 \pm 0.02$	$-0.04 \pm 0.01$	$-0.048 \pm 0.002$

A detailed higher-twist analysis based on the combined SLAC and JLab data [on proton, neutron  $\Gamma_1^{p,n}(Q^2)$  [33] and nonsinglet  $\Gamma_1^{p-n}(Q^2)$  moments [35]] was performed in Refs. [35–38]. In Table II, we show the current results for the twist-4 coefficient  $\mu_4/M^2$  at  $Q^2 = 1$  GeV<sup>2</sup> extracted from  $\Gamma_1^{p,n}$  data. As we have seen from our previous analysis [6], a satisfactory description of the low-energy JLab data on the Bjorken sum rule down to  $Q_{min} \sim \Lambda_{QCD} \simeq 350$  MeV can be achieved by using APT and taking into account only three higher-twist terms  $\mu_{4,6,8}^{p-n}$ . Including only the twist-4 term  $\mu_4^{p-n}/M^2$ , this method allowed us to get its value with noticeably higher accuracy than in the standard PT approach, shifting the applicability of the pQCD expansion down to  $Q_{min}^2 = 0.47$  GeV<sup>2</sup>. The higher-twist analysis of the most recent precise JLab experimental data on the proton spin sum rule [20] has not been carried out yet in the literature. This gives us a reasonable motivation for a detailed data analysis and studying the higher-twist effects at low-energy scale both in the standard PT, APT and “infrared-frozen”  $\alpha_s$  approaches.

## B. The running coupling

The infrared behavior of the strong coupling is crucial for the extraction of the nonperturbative information from the low-energy data. Within the pQCD, the  $\alpha_s$  coupling can be found by a solution of the RG equation

$$\frac{d\alpha_s}{dL} = -\beta_0\alpha_s^2(1 + b_1\alpha_s + b_2\alpha_s^2 + \dots),$$

where  $L = \ln(Q^2/\Lambda^2)$  and  $b_k = \beta_k/\beta_0$ . The standard PT running coupling  $\alpha_s$  is usually taken in the form [see, for example, Eq. (6) in the recent review [39] or Eq. (9.5) in the PDG review [13]] expanded in a series over  $\ln L/L$ , i.e.

$$\alpha_s^{(3)}(L) = \frac{1}{\beta_0 L} - \frac{b_1 \ln L}{\beta_0^2 L^2} + \frac{1}{\beta_0^3 L^3} [b_1^2(\ln^2 L - \ln L - 1) + b_2]. \quad (2.9)$$

Here, the  $1/L^2$  term corresponds to the 2-loop contribution and the  $1/L^3$  term is usually referred to as “the 3-loop one.” Actually, the pieces of genuine 2-loop contribution proportional to  $b_1$  are entangled with the higher-loop ones. This defect is absent in the more compact denominator representation [12], which at 2, 3-loop levels has the following forms:

$$\frac{1}{\alpha_s^{(2),D}(L)} = \beta_0 L + b_1 \ln \left( L + \frac{b_1}{\beta_0} \right), \quad \frac{1}{\alpha_s^{(3),D}(L)} = \beta_0 L + b_1 \ln \left( L + \frac{b_1}{\beta_0} \ln L \right) + \frac{b_1^2 - b_2}{\beta_0 L}, \quad (2.10)$$

which, being generic for the PDG expression (2.9), are closer to the corresponding iterative RG solutions and, hence, more precise. Advantages of formulas (2.10) in the higher-twist analysis of the Bjorken sum rule were demonstrated in our previous work [6].

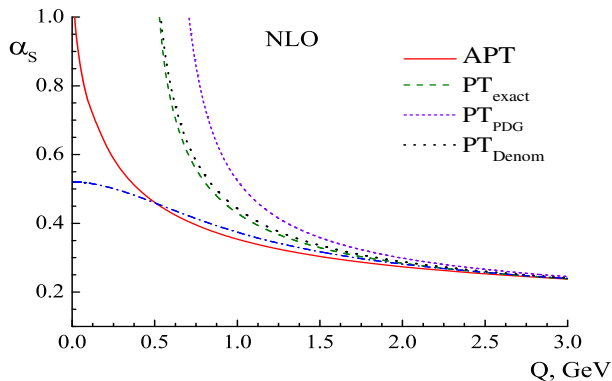


FIG. 1: The NLO running coupling  $\alpha_s$  in different approaches.

In Fig. 1, we compare the behavior of the two-loop running coupling  $\alpha_s$  at low  $Q^2$  scales in different approaches. The long-dashed line is the exact two-loop PT result, the dotted line is the denominator representation (2.10) (referred to as “Denom” below), and the short-dashed line is the PDG expression (2.9). As one can see from this figure, the NLO Denom coupling is much closer to the corresponding numerical RG solution than the  $1/L$ -expanded PDG expression.

In Fig. 1, we also show two models of the infrared-stable running coupling. One of them is the Simonov “glueball-freezing model” (SGF-model) [17], represented by the dash-dotted line, with the  $1/L$ -type loop expansion for the “infrared-frozen” coupling similar to PDG

$$\alpha_B(Q^2) = \alpha_s^{(2)}(\bar{L}), \quad \bar{L} = \ln\left(\frac{Q^2 + M_0^2}{\Lambda^2}\right), \quad (2.11)$$

where the two-loop  $\alpha_s^{(2)}$  is taken in the form of the first two terms in Eq. (2.9) with logarithm modified by a “glueball mass”  $M_0 \sim 1$  GeV. Note, the usual PT expansion in powers of  $\alpha_B$  in the coefficient functions (2.3) and (2.4) is adopted. The solid line corresponds to the second model of the infrared-stable coupling – the APT running coupling, which will be discussed in detail below in the next section.

As one can see from Fig. 1, the SGF and APT couplings are very similar in the low-energy domain  $\Lambda_{QCD} < Q \lesssim 1$  GeV though their infrared limits are different. Also, a comparison of APT and PT couplings over a wide range of  $Q^2$ ,  $1 \leq Q^2 \leq 10^4$  GeV<sup>2</sup>, can be found in Ref. [40].

Note, we extract values of  $\Lambda_{QCD}$  corresponding to different models of the running coupling, by evolution from the world experimental data on  $\alpha_s(M_Z^2)$  as a normalization point in each particular order of PT.

### C. Stability and duality

In the following, when calculating the observables in any particular order of perturbation theory, we will employ the prescription for the coefficient functions in the infrared region, where the order of the power  $\alpha_s$  series in the coefficient functions is matched with the loop order in  $\alpha_s$  itself. For example, for the nonsinglet coefficient function in the Bjorken sum rule, we write consequently (for details, see Ref. [29])

$$E_{NS}^{LO} = 1, \quad E_{NS}^{NLO} = 1 - \frac{\alpha_s^{NLO}}{\pi}, \quad E_{NS}^{N^2LO} = 1 - \frac{\alpha_s^{N^2LO}}{\pi} - 3.558 \left(\frac{\alpha_s^{N^2LO}}{\pi}\right)^2, \dots \quad (2.12)$$

We see that the leading singular behavior in the coefficient function  $\sim \ln^n L/L^m$  when  $L \rightarrow 0$  comes from the highest power of  $\alpha_s$ . So in the infrared domain the influence of singularities gets stronger in higher orders of perturbation theory that may affect the data analysis below 1 GeV<sup>2</sup>. This fact explains our observation made in Ref. [6], where we showed that the higher PT orders yield a worse description of the BSR data in comparison with the leading order. We observe a similar picture for the precise JLab data on  $\Gamma_1^p(Q^2)$  [20] probably implying the asymptotic character of the series in powers of  $\alpha_s$  (see Fig. 2).

The corresponding fit results for HT terms, extracted in different orders of PT, are listed in Table III. We see that with raising the loop order the values of  $\mu_{4,8}^p$  terms increase, whereas  $\mu_6^p$  decreases, yielding a “swap” between the higher orders of PT and HT terms. Such a “swap” between PT and HT terms (decreasing HT term by including more terms of PT and using resummation of PT series) was previously observed in Refs. [41, 42]. A similar situation holds when fitting  $\Gamma_1^p(Q^2)$  data over the fixed range  $0.8 \text{ GeV} < Q < 2.0 \text{ GeV}$ , where it is sufficient to take into account only one twist term  $\mu_4$ .

In Fig. 3, we show fits of BSR data (left panel) and proton SSR data (right panel) in different orders of perturbation theory taking only into account the  $\mu_4$  term. One can see there that the higher-loop contributions are effectively “absorbed” into the value of  $\mu_4$  which

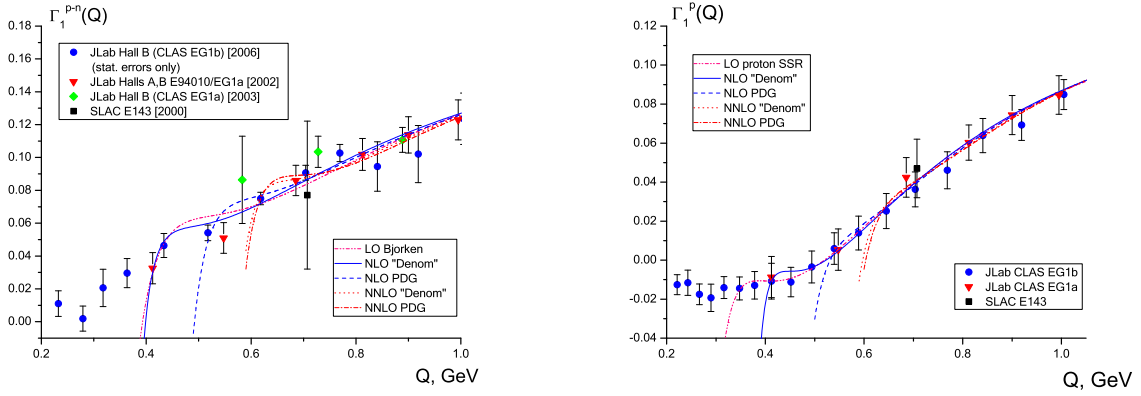


FIG. 2: Best fits of JLab and SLAC data on BSR  $\Gamma_1^{p-n}(Q^2)$  (left panel) and proton SSR  $\Gamma_1^p(Q^2)$  (right panel) calculated at various loop orders.

TABLE III: Dependence of the best fit results of BSR  $\Gamma_1^{p-n}(Q^2)$  and proton SSR  $\Gamma_1^p(Q^2)$  data (elastic contribution excluded) on the order of perturbation theory [NLO and NNLO Denom couplings (2.10) are used]. The corresponding fit curves are shown in Fig. 2. The minimal borders of fitting domains in  $Q^2$  are settled from the *ad hoc* restriction  $\chi^2 \leq 1$  and monotonous behavior of the resulting fitted curves.

Target	Method	$Q_{min}^2, \text{ GeV}^2$	$a_0^{inv}$	$\mu_4/M^2$	$\mu_6/M^4$	$\mu_8/M^6$
proton	LO	0.121	0.29(2)	-0.089(3)	0.016(1)	-0.0010(1)
	NLO	0.17	0.38(2)	-0.070(5)	0.010(2)	0.0004(3)
	NNLO	0.38	0.37(5)	-0.034(19)	-0.025(20)	0.017(6)
p - n	LO	0.17	-	-0.126(5)	0.037(3)	-0.004(1)
	NLO	0.17	-	-0.076(5)	0.019(3)	-0.001(1)
	NNLO	0.38	-	-0.026(11)	-0.035(15)	0.026(5)

decreases in magnitude with increasing loop order while all the fitting curves are very close to each other. This observation reveals a kind of “duality” between the perturbative  $\alpha_s$  series and nonperturbative  $1/Q^2$  series. A similar phenomenon was observed before for the structure function  $F_3$  in Refs. [43, 44].

This also means the appearance of a new aspect of quark hadron duality, the latter being the necessary ingredient of all the QCD applications in the low-energy domain. Usually, it is assumed [45] that the perturbative effects are less important there than the power ones due to a nontrivial structure in the QCD vacuum.

In our case, the PT corrections essentially enter into the game, so that the pQCD higher order terms are relevant in the domain where the concepts of traditional hadronic physics are usually applied.

The interplay between partonic and hadronic degrees of freedom in the description of GDH SR and BSR may also be observed in the surprising similarity between the results of “resonance” [46] and “parton” [9] approaches.

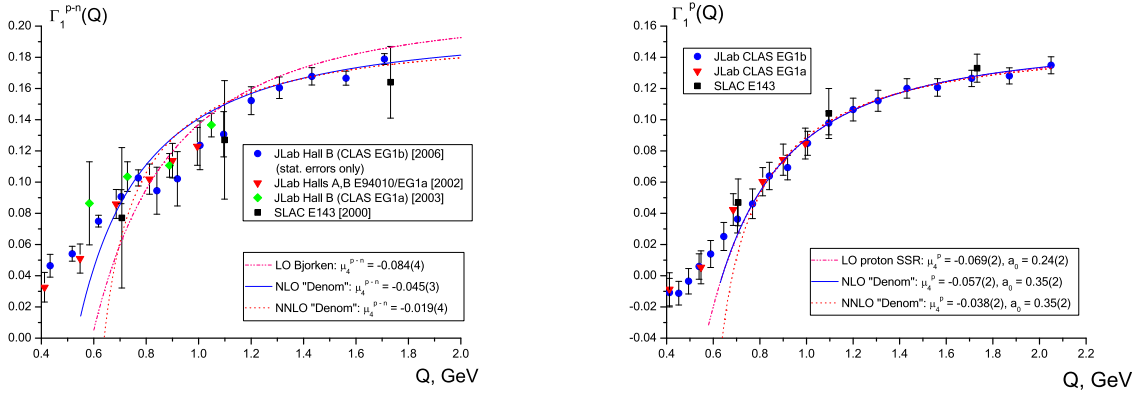


FIG. 3: Best fits of JLab and SLAC data on BSR  $\Gamma_1^{p-n}(Q^2)$  (left panel) and proton SSR  $\Gamma_1^p(Q^2)$  (right panel) calculated in various loop orders with fixed  $Q_{min} = 0.8$  GeV.

TABLE IV: Dependence of the best  $(3+1)$ -parametric fit results of  $\Gamma_1^p(Q^2)$  data (elastic contribution excluded) on  $\Lambda_{n_f=3}$  in NLO Denom PT.

$\Lambda_{QCD}$ , MeV	$Q_{min}^2$ , GeV <sup>2</sup>	$a_0^{inv}$	$\mu_4/M^2$	$\mu_6/M^4$	$\mu_8/M^6$
300	0.14	0.40(2)	-0.077(3)	0.014(1)	-0.0005(2)
400	0.24	0.39(3)	-0.064(8)	0.006(5)	0.002(1)
500	0.35	0.34(4)	-0.028(13)	-0.033(11)	0.019(3)

One may ask to what extent these results are affected by the unphysical singularities when approaching  $Q \sim \Lambda_{QCD}$  in the PT series for  $\Gamma_{1,PT}^{p,n}$ . Their influence becomes essential at  $Q < 1$  GeV where the HT terms start to play an important role. The minimal border of the fitting domain  $Q_{min}$  is tightly connected with the value of  $\Lambda_{QCD}$ ; i.e. it is a scale, below which the influence of the ghost singularities becomes too strong and destroys the fit. To see how the  $Q_{min}^2$  scale and fit results for the  $\mu$  terms change with varying  $\Lambda_{QCD}$ , we have performed three different NLO fits with  $\Lambda_{QCD} = 300, 400, 500$  MeV (see Table IV). It turns out that the term  $\mu_4$  is quite sensitive to the Landau singularity position, and its value noticeably increases with increasing  $\Lambda_{QCD}$ . The APT and “soft-frozen” models are free of such a problem, thus providing a reliable tool of investigating the behavior of HT terms extracted directly from the low-energy data [6]. This provides a motivation for the analysis performed in the next section.

### III. MOMENTS $\Gamma_1^{p,n}(Q^2)$ IN ANALYTIC PERTURBATION THEORY

The moments of the structure functions are analytic functions in the complex  $Q^2$  plane with a cut along the negative real axis, as was demonstrated in Ref. [47] (see also Ref. [48]). On the other hand, the standard PT approach does not support these analytic properties. The influence of requiring these properties to hold in the DIS description was studied previ-

ously by Igor Solovtsov and coauthors in Refs. [40, 49]. Here we continue this investigation by applying the APT method, which gives the possibility of combining the RG resummation with correct analytic properties of the QCD corrections, to the low-energy data on nucleon spin sum rules  $\Gamma_1^{p,n}(Q^2)$ .

In the framework of the analytic approach we can write the expression for  $\Gamma_1^{p,n}(Q^2)$  in the form

$$\Gamma_{1,APT}^{p,n}(Q^2) = \frac{1}{12} \left[ \left( \pm a_3 + \frac{1}{3} a_8 \right) E_{NS}^{APT}(Q^2) + \frac{4}{3} a_0^{inv} E_S^{APT}(Q^2) \right] + \sum_{i=2}^{\infty} \frac{\mu_{2i}^{APT;p,n}(Q^2)}{Q^{2i-2}}, \quad (3.1)$$

which is analogous to one in the standard PT (2.2). The corresponding NNLO APT modification of the singlet and nonsinglet coefficient functions is

$$E_{NS}^{APT}(Q^2) = 1 - 0.318 \mathcal{A}_1^{(3)}(Q^2) - 0.361 \mathcal{A}_2^{(3)}(Q^2) - \dots, \quad (3.2)$$

$$E_S^{APT}(Q^2) = 1 - 0.318 \mathcal{A}_1^{(3)}(Q^2) - 0.111 \mathcal{A}_2^{(3)}(Q^2) - \dots, \quad (3.3)$$

where  $\mathcal{A}_k^{(3)}$  is the analyticized  $k$ th power of 3-loop PT coupling in the Euclidean domain

$$\mathcal{A}_k^{(n)}(Q^2) = \frac{1}{\pi} \int_0^{+\infty} \frac{\text{Im}([\alpha_s^{(n)}(-\sigma, n_f)]^k) d\sigma}{\sigma + Q^2}, \quad n = 3. \quad (3.4)$$

In the one-loop case, the APT Euclidean functions are simple enough [14]:

$$\mathcal{A}_1^{(1)}(Q^2) = \frac{1}{\beta_0} \left[ \frac{1}{L} + \frac{\Lambda^2}{\Lambda^2 - Q^2} \right], \quad L = \ln \left( \frac{Q^2}{\Lambda^2} \right), \quad (3.5)$$

$$\mathcal{A}_2^{(1)}(l) = \frac{1}{\beta_0^2} \left[ \frac{1}{L^2} - \frac{Q^2 \Lambda^2}{(Q^2 - \Lambda^2)^2} \right], \quad \mathcal{A}_{k+1}^{(1)} = -\frac{1}{k \beta_0} \frac{d\mathcal{A}_k^{(1)}}{dL},$$

i.e. the higher functions  $\mathcal{A}_k$  are related to the lower ones recursively by differentiating. Analogous two- and three-loop level expressions involve the special Lambert function and are more intricate, and they can be found in Refs. [50, 51]. It should be stressed that the APT couplings are stable with respect to different loop orders at low-energy scales  $Q^2 \lesssim 1 \text{ GeV}^2$  [15]. This feature is absent in the standard PT approach, as reflected in Fig. 2.

Meanwhile, even for the three-loop APT case, there exists a possibility to employ *the effective log approach* proposed by Igor Solovtsov and one of the authors in Ref. [52]. In the present context, in the region  $Q < 5 \text{ GeV}$  one may use simple model one-loop expressions (3.5) with some *effective logarithm*  $L^*$ :

$$\mathcal{A}_{1,2,3}^{(3)}(L) \rightarrow \mathcal{A}_{1,2,3}^{mod} = \mathcal{A}_{1,2,3}^{(1)}(L^*), \quad L^* \simeq 2 \ln(Q/\Lambda_{eff}^{(1)}), \quad \Lambda_{eff}^{(1)} \simeq 0.50 \Lambda^{(3)}. \quad (3.6)$$

Thus, instead of the exact three-loop expressions for the APT functions, in Eq. (3.3) one can use the one-loop expressions (3.5) with the effective  $\Lambda$  parameter  $\Lambda_{mod} = \Lambda_{eff}^{(1)}$  whose value is given by the last relation (3.6). This model was successfully applied for higher-twist analysis of low-energy data on BSR in our previous work [6], and also in the  $\Upsilon$  decay analysis in Ref. [53].

The maximal errors of the model (3.6) for the first and the second functions are  $\delta \mathcal{A}_1^{mod}/\mathcal{A}_1^{mod} \simeq 4\%$  and  $\delta \mathcal{A}_2^{mod}/\mathcal{A}_2^{mod} \simeq 8\%$  at  $Q \sim \Lambda_{n_f=3}$ , which seem to be sufficiently accurate. Indeed, as far as  $\mathcal{A}_1(Q = 400 \text{ MeV}) = 0.532$  and  $\mathcal{A}_2(400 \text{ MeV}) = 0.118$ ,

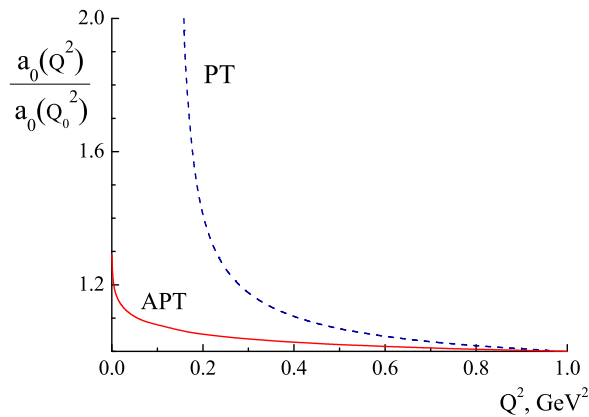


FIG. 4: Evolution of  $a_0(Q^2)$  normalized at  $Q_0^2 = 1 \text{ GeV}^2$ .

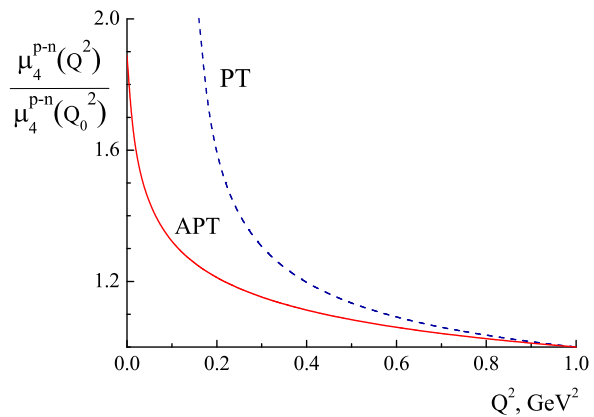


FIG. 5: Evolution of  $\mu_4^{p-n}(Q^2)$  normalized at  $Q_0^2 = 1 \text{ GeV}^2$ .

the total error in  $\Gamma_{1,\text{APT}}^p$  is mainly determined by the first term, being of the order  $\delta\Gamma_1^p/\Gamma_1^p \simeq \delta\mathcal{A}_1^{\text{mod}}/\pi \sim 1\%$ , i.e., less than the data uncertainty.

In order to take into account the one-loop  $Q^2$  evolution of the axial singlet charge  $a_0(Q^2)$ , we use expression (2.9) substituting the one-loop analytic coupling  $\mathcal{A}_1^{(1)}(L)$ . The contribution of the  $\sim \mathcal{A}_1$  term to  $a_0(Q^2)$  at, for example,  $Q^2 = 0.1 \text{ GeV}^2$  with normalization point at  $Q_0^2 = 1 \text{ GeV}^2$  is  $\Delta_1(0.1 \text{ GeV}^2) \simeq 0.11$ ; i.e. the evolution contributes about 10% when one shifts the pQCD border down to  $\Lambda_{QCD}$  (see Fig. 4).

For the evolution of the twist-4 term  $\mu_4(Q^2)$  (2.7), we have to “analyticize” the fractional power  $(\alpha_s)^\nu$ . For this purpose we apply the fractional APT approach developed in Ref. [54]. At the one-loop level in the Euclidean domain we have

$$\mathcal{A}_\nu^{(1)}(L) = \frac{1}{L^\nu} - \frac{F(e^{-L}, 1 - \nu)}{\Gamma(\nu)}. \quad (3.7)$$

Here  $F(z, \nu)$  is the Lerch transcendent function. In this case, the evolution of the nonsinglet twist-4 term in BSR reads

$$\mu_{4,\text{APT}}^{p-n}(Q^2) = \mu_{4,\text{APT}}^{p-n}(Q_0^2) \frac{\mathcal{A}_\nu^{(1)}(Q^2)}{\mathcal{A}_\nu^{(1)}(Q_0^2)}, \quad \nu = \frac{32}{81}. \quad (3.8)$$

The corresponding evolution is shown in Fig. 5. As follows from this figure, the evolution from 1 GeV to  $\Lambda_{QCD}$  increases the absolute value of  $\mu_{4,\text{APT}}^{p-n}$  by about 20 %.

## IV. NUMERICAL RESULTS

### A. Nonsinglet case: the Bjorken sum rule

In Fig. 6, we show best fits of the combined data set for the BSR function  $\Gamma_1^{p-n}(Q^2)$  with NLO Denom (solid lines) and PDG (dashed lines) couplings and NNLO APT (dash-dotted lines) at fixed  $\Lambda_{QCD}$  value corresponding to the world average. We also show here the

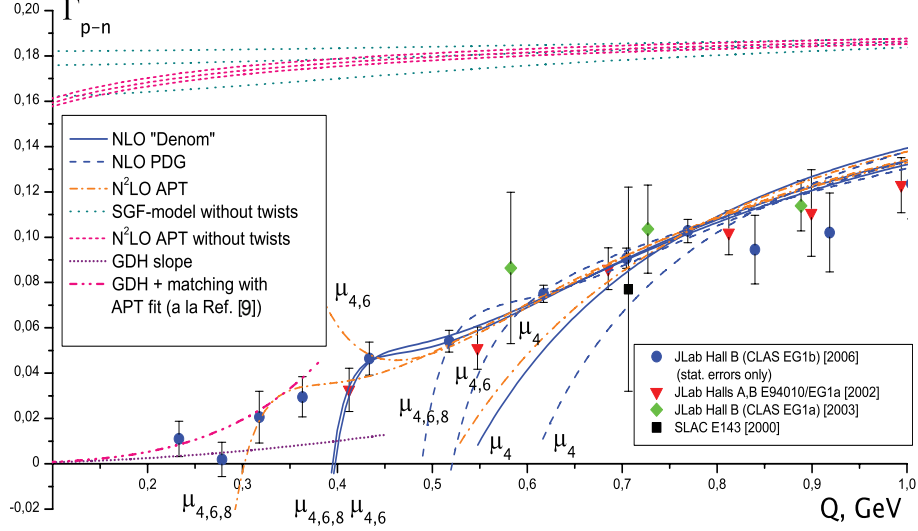


FIG. 6: Best 1,2,3-parametric fits of the JLab and SLAC data on Bjorken SR calculated with different models of running coupling.

TABLE V: Combined fit results of BSR for the HT terms in APT, the SGF model and the standard PT approach.

Method	$Q_{min}^2, \text{ GeV}^2$	$\mu_4/M^2$	$\mu_6/M^4$	$\mu_8/M^6$
NLO PDG	0.50	-0.043(3)	0	0
	0.30	-0.074(3)	0.026(7)	0
	0.27	-0.049(4)	-0.010(3)	0.010(1)
NLO Denom	0.47	-0.049(3)	0	0
	0.17	-0.069(4)	0.014(1)	0
	0.17	-0.065(7)	0.011(3)	0.0003(7)
NLO SGF	0.47	-0.061(3)	0	0
	0.19	-0.073(3)	0.010(3)	0
	0.10	-0.077(4)	0.014(5)	-0.0008(3)
NNLO APT no evolution	0.47	-0.055(3)	0	0
	0.17	-0.062(4)	0.008(2)	0
	0.10	-0.068(4)	0.010(3)	-0.0007(3)
NNLO APT with evolution	0.47	-0.051(3)	0	0
	0.17	-0.056(4)	0.0087(4)	0
	0.10	-0.058(4)	0.0114(6)	-0.0005(8)

pQCD part of the BSR at different values of  $\Lambda_{QCD} = 300, 400, 500$  MeV calculated within APT (short-dashed lines) and the SGF model [17] at different values of the glueball mass  $M_0 = 1.2, 1.0, 0.8$  GeV (with  $\Lambda = 360$  MeV) (dotted lines).

The corresponding numerical results are given in Table V. As we have seen before in Fig. 1, the behavior of SGF and APT couplings is very similar in the low-energy domain

$\Lambda_{QCD} < Q \lesssim 1$  GeV. As a result, the corresponding perturbative parts of BSR in Fig. 6 and results for higher-twist terms in Table V turn out to be close, too. Our fits in APT and the SGF model give the HT values indicating a better convergence of the OPE series due to decreasing magnitudes and alternating signs of consecutive terms, in contrast to the usual PT fit results.

As is seen from Table V, there is some sensitivity of fitted values of  $\mu_4$  with respect to  $Q_{min}$  variations; namely, it increases in magnitude when one incorporates into the fit the data points at lower energies. This property of the fit may be treated as the slow (logarithmic) evolution  $\mu_4(Q^2)$  with  $Q^2$  which becomes more noticeable at broader fitting ranges in  $Q^2$ , as discussed above. So for completeness we included in Table V APT fits for  $\mu_4(Q_0^2)$  taking into account their RG evolution with  $Q_0 = 1$  GeV as a normalization point. We see that the fit results become more stable with respect to  $Q_{min}$  variations.

However, there is still a problem with how to treat the evolution of higher-twist terms  $\mu_{6,8,\dots}(Q^2)$  which again may turn out to be important when one goes to lower  $Q^2$ , since the fit becomes more sensitive to very small variations of  $\mu_{6,8,\dots}$  with  $Q^2$ .

Note that the APT functions  $\mathcal{A}_k$  contain the  $(Q^2)^{-k}$  power contributions which effectively change the fitted values of  $\mu$  terms. In particular, subtracting an extra  $(Q^2)^{-1}$  term induced by the APT series

$$\Gamma_{1,APT}^{p-n}(Q^2) \simeq \frac{g_A}{6} + f \left( \frac{1}{\ln(Q^2/\Lambda_{eff}^{(1)2})} \right) + \varkappa \frac{\Lambda_{eff}^{(1)2}}{Q^2} + \mathcal{O} \left( \frac{1}{Q^4} \right)$$

with  $\varkappa = 0.43$  and using the value  $\mu_{4,APT}^{p-n}/M^2 = -0.058$  (with evolution) from Table V, we finally get

$$\frac{\mu_{4,APT}^{p-n} + \varkappa \Lambda_{eff}^{(1)2}}{M^2} \simeq \frac{\mu_4^{p-n}(1 \text{ GeV}^2)}{M^2} \simeq -0.042, \quad \Lambda_{eff}^{(1)} \sim 0.18 \text{ GeV} \quad (4.1)$$

that nicely correlates with the result in Ref. [35]:  $\mu_4^{p-n}/M^2 \simeq -0.045$ . This demonstrates the concert of the APT analysis with the usual PT one for the BSR data at  $Q^2 \geq 1$  GeV<sup>2</sup>.

We do not take into account RG evolution in  $\mu_4$  for the standard PT calculations since the only effect of that would be the enhancement of the Landau singularities by extra divergencies at  $\Lambda_{QCD}$  (see Fig. 5), whereas at higher  $Q^2 \sim 1$  GeV<sup>2</sup> the evolution is negligible with respect to other uncertainties. In ghost-free models, however, the evolution gives a noticeable effect at low  $Q \sim \Lambda_{QCD}$ . Note that our previous result in Ref. [6], obtained without taking into account the RG evolution, turned out to be slightly larger than (4.1)  $\mu_4^{p-n}/M^2 \simeq -0.048$  which is very close to the corresponding value obtained with the most precise Denom PT coupling and is shown in Table V.

## B. Singlet case: spin sum rules $\Gamma_1^{p,n}$ and nucleon spin structure

Turn now to the three-loop APT part of the proton moment  $\Gamma_{1,APT}^p(Q^2)$ . Its value is quite stable with respect to small variations of  $\Lambda$ , in contrast to the huge instability of  $\Gamma_{1,PT}^p$ : it changes now by about 2% – 3% within the interval  $\Lambda^{(3)} = 300 - 500$  MeV. The same was previously observed for the Bjorken function  $\Gamma_{1,APT}^{p-n}(Q^2)$  in Ref. [6]. Because of this fact the low- $Q^2$  data on  $\Gamma_1^p(Q^2)$  cannot be used for determination of  $\Lambda$  in the APT approach.

Extending the analysis of Ref. [49] to lower  $Q^2$  scales, we estimated the relative size of APT contributions to  $\Gamma_1^p(Q^2)$ . It turned out that the third term  $\sim \mathcal{A}_3$  contributes no more than 5% to the sum, thus supporting the practical convergence of the APT series.

TABLE VI: Sensitivity of the best APT fit results of proton  $\Gamma_1^p(Q^2)$  data (elastic contribution excluded) to  $\Lambda_{n_f=3}$  variations. The minimal fitting border is  $Q_{min}^2 = 0.12 \text{ GeV}^2$ .

$\Lambda_{QCD}, \text{ MeV}$	$a_0^{inv}$	$\mu_4/M^2$	$\mu_6/M^4$	$\mu_8/M^6$
300	0.43(3)	-0.082(4)	0.015(9)	-0.0009(5)
400	0.45(3)	-0.081(4)	0.015(9)	-0.0009(5)
500	0.47(3)	-0.080(4)	0.014(9)	-0.0009(5)

To see how the numerical fit results are sensitive to  $\Lambda_{(n_f=3)}$  in APT, we fulfilled four different fits of the proton  $\Gamma_1^p(Q^2)$  data with  $\Lambda_{QCD} = 300, 400, 500 \text{ MeV}$  as we did before in the standard PT. The results of these fits are shown in Table VI. Comparing these results with the data from Table IV, we see that the corresponding results in the standard PT are much more sensitive to  $\Lambda$  variations than ones in APT.

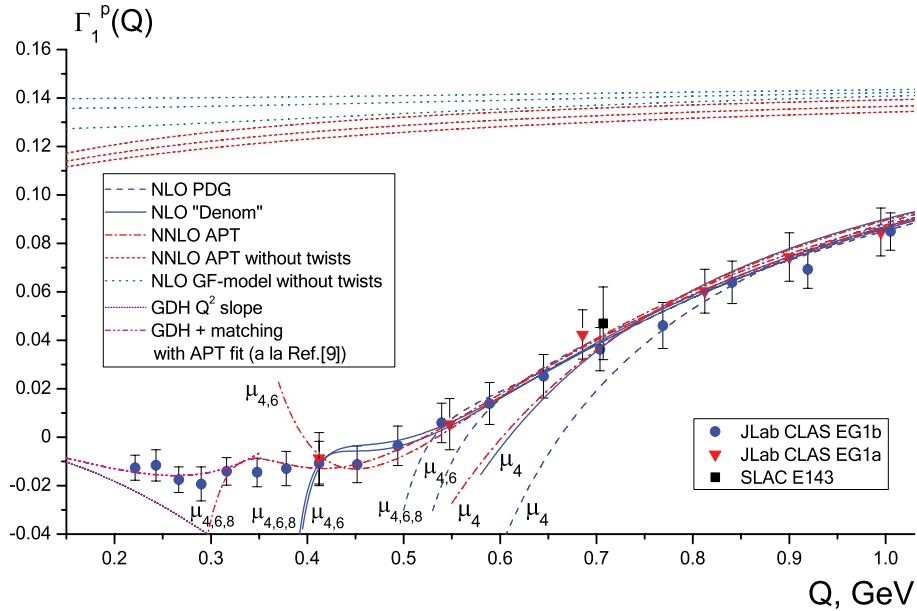


FIG. 7: Best (1,2,3+1)-parametric fits of the JLab and SLAC data on  $\Gamma_1^p$  (elastic contribution excluded).

In Fig. 7, we show best fits of the combined data set for the function  $\Gamma_1^p(Q^2)$  (the data uncertainties are statistical only) in the standard PT (PDG and Denom versions) and the APT approaches. We have also shown the perturbative parts of  $\Gamma_1^p(Q^2)$  calculated in APT and the SGF model. They are close to each other down to  $Q \sim \Lambda$ , similar to the BSR analysis in the previous subsection. A similar observation was made in the analysis of the small  $x$  spin averaged structure functions in Ref. [34].

In Table VII, we present the combined fit results of the proton  $\Gamma_1^p(Q^2)$  data (elastic contribution excluded) in APT, the SGF model and conventional PT in PDG and denominator

forms. One can see there is noticeable sensitivity of the extracted  $a_0^{inv}$  and  $\mu_4$  with respect to the minimal fitting scale  $Q_{min}^2$  variations, which may be (at least, partially) compensated by their RG  $\log Q^2$  evolution, similar to the BSR case. For completeness we included in Table VII APT fits for  $a_0^{inv}(Q_0^2)$  and  $\mu_4(Q_0^2)$ , taking into account their RG evolution.

TABLE VII: Combined fit results of the proton  $\Gamma_1^p(Q^2)$  data (elastic contribution excluded). APT fit results  $a_0$  and  $\mu_{4,6,8}^{APT}$  (at the scale  $Q_0^2 = 1 \text{ GeV}^2$ ) are given without and with taking into account the RG  $Q^2$  evolution of  $a_0(Q^2)$  and  $\mu_4^{APT}(Q^2)$ .

Method	$Q_{min}^2, \text{ GeV}^2$	$a_0$	$\mu_4/M^2$	$\mu_6/M^4$	$\mu_8/M^6$
NLO PDG	0.59	0.33(3)	-0.050(4)	0	0
	0.35	0.43(5)	-0.087(9)	0.024(5)	0
	0.29	0.37(5)	-0.060(15)	-0.001(8)	0.006(5)
NLO Denom	0.59	0.35(3)	-0.058(4)	0	0
	0.20	0.38(3)	-0.076(4)	0.013(1)	0
	0.17	0.38(4)	-0.070(8)	0.010(4)	0.0004(5)
NLO SGF $M_0 = 1 \text{ GeV}$	0.47	0.32(4)	-0.056(4)	0	0
	0.17	0.36(3)	-0.071(4)	0.0082(9)	0
	0.10	0.40(4)	-0.080(4)	0.0134(9)	-0.0007(6)
NNLO APT no evolution	0.47	0.35(4)	-0.054(4)	0	0
	0.17	0.39(3)	-0.069(4)	0.0081(8)	0
	0.10	0.43(3)	-0.078(4)	0.0132(9)	-0.0007(5)
NNLO APT with evolution	0.47	0.33(4)	-0.051(4)	0	0
	0.17	0.31(3)	-0.059(4)	0.0098(8)	0
	0.10	0.32(4)	-0.065(4)	0.0146(9)	-0.0006(5)

As we already mentioned, the evolution of the  $\mu_4^p(Q^2)$  is taken to be the same as for the nonsinglet term  $\mu_4^{p-n}(Q^2)$ , allowing one to keep only one fitting parameter  $\mu_4^p(Q_0^2)$  instead of two in the general case. We also tested that the singlet anomalous dimension instead of the nonsinglet one [resulting in the same  $Q^2$  evolution of  $\mu_4^p(Q^2)$  as that of  $\mu_4^{p+n}(Q^2)$ ] leads to close fit results within error bars.

Figure 8 demonstrates the characteristic values of the proton data fits  $\chi^2/D.o.f.$  (upper row) and the twist-4 coefficient  $\mu_4$  (lower row) as functions of  $a_0$  at different values of  $Q_{min}^2$  (numbers at the curves). One can see that at lower  $Q^2$  ( $Q_{min}^2 < 1 \text{ GeV}^2$ ) the APT description (left panels) turns out to be more precise and stable than that in the standard PT (right panels). Though we have taken the fitted values of  $a_0$  and higher twists  $\mu_{2i}$  in the minima of each  $\chi^2/D.o.f.$  curve as best fits, the naive constraint  $\chi^2/D.o.f. \leq 1$  (dotted horizontal lines mark 1) provides a quite wide spread in the allowable values of the fit parameters. However, it would be reasonable to take the spread between different minima as an optimistic error bar of our analysis. This gives us the following result:  $a_0 = 0.33 \pm 0.05$ , which is consistent with the recent analysis by COMPASS [28] and HERMES [29] (see Table I).

In Fig. 9, we show the best fit results for the less precise neutron  $\Gamma_1^n(Q^2)$  data. Again, the APT fit gives the HT values demonstrating a better convergence of the OPE series, in contrast to the usual PT fit results. Fits with APT and more precise Denom PT couplings

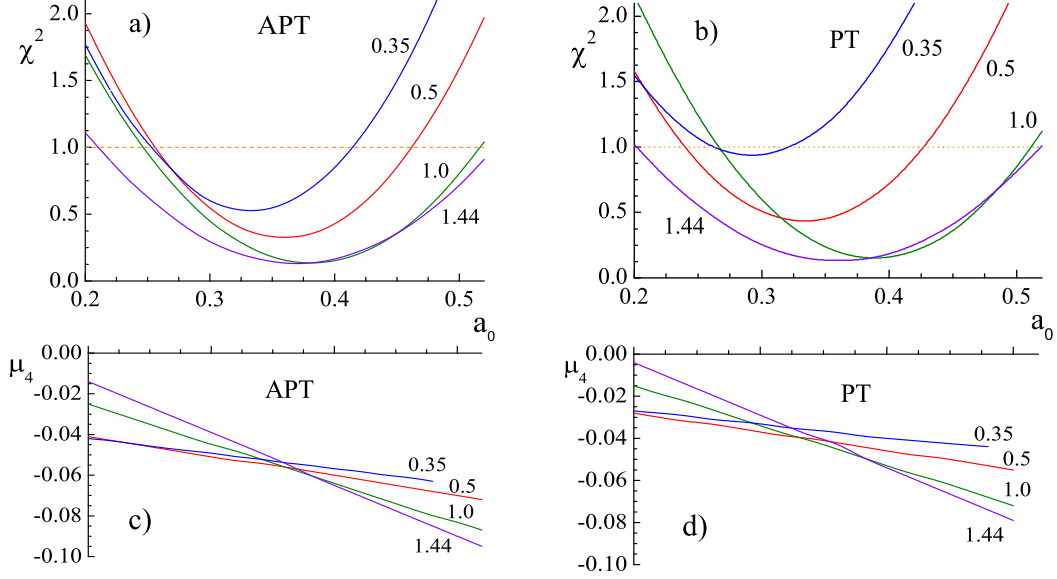


FIG. 8: Behavior of  $\chi^2/D.o.f.$  and  $\mu_4^p$  from the proton data fits (with only one  $1/Q^2$  term) as functions of  $a_0$  at different values of  $Q_{min}^2$  (the numbers at the curves) in the APT (left panels) and PT (right panels) cases.

lead to a much smaller value of  $\mu_4^n$  and more stable fitting curves than that with the PDG coupling. Also the axial singlet charge  $a_0$  extracted within APT from the neutron data turns out to be very close to the one extracted from more precise proton data (see Table VII).

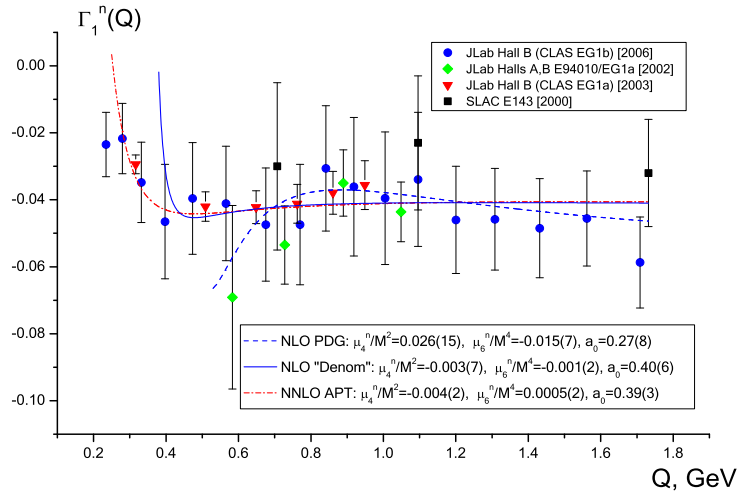


FIG. 9: Best (2+1)-parametric fits of the JLab and SLAC data on  $\Gamma_1^n$  calculated with NLO Denom (solid line) and PDG (dashed line) couplings and NNLO APT (dash-dotted line).

To obtain the genuine value of the twist-4 term  $\mu_4^p$ , we act in a similar way as for the BSR case in the previous subsection, namely, subtracting an extra  $(Q^2)^{-1}$  term induced by

the APT series

$$\begin{aligned}
E_{NS}^{APT}(Q^2) &= E_{NS}(\alpha_s = \alpha_s^{LO}(Q^2)) + \varkappa_4^{NS} \frac{\Lambda_{eff}^{(1)2}}{Q^2} + \mathcal{O}\left(\frac{1}{Q^4}\right), \\
E_S^{APT}(Q^2) &= E_S(\alpha_s = \alpha_s^{LO}(Q^2)) + \varkappa_4^S \frac{\Lambda_{eff}^{(1)2}}{Q^2} + \mathcal{O}\left(\frac{1}{Q^4}\right)
\end{aligned}
\tag{4.2}$$

with  $\Lambda_{eff}^{(1)} \sim 0.18$  GeV,  $\varkappa_4^{NS} = 2.035$ , and  $\varkappa_4^S = 0.661$ , and using the fit result in APT (with evolution)  $\mu_4^{p,APT}/M^2 = -0.065$  from Table VII, we obtain

$$\frac{\mu_4^p(1 \text{ GeV}^2)}{M^2} \simeq \frac{1}{M^2} \left( \mu_4^{p,APT} + \frac{1}{12} \left( a_3 + \frac{1}{3} a_8 \right) \varkappa_4^{NS} \Lambda_{eff}^{(1)2} + \frac{1}{9} a_0^{inv} \varkappa_4^S \Lambda_{eff}^{(1)2} \right) \simeq -0.055. \tag{4.3}$$

Analogously, for a neutron we have  $\mu_4^n/M^2 \simeq -0.010$ . Subtracting it from the proton value (4.3), we get for the nonsinglet twist-4 term  $\mu_4^{p-n}/M^2 \simeq -0.045$ , which is close to the result in Ref. [38], showing up the consistence of the APT analysis with the usual PT one for the proton and neutron SSR  $\Gamma_1^{p,n}$  data at  $Q^2 \geq 1$  GeV<sup>2</sup>. Our result (4.3) is also consistent with the previous extraction at higher energies in Ref. [36] within the error bars (see also Table II).

It is worth noting that the best APT fit allows one to describe low-energy JLab data on  $\Gamma_1^{p,n}$  at scales down to  $Q \sim 350$  MeV with only the first three terms of the OPE series, unlike the usual PT case, where such fits happened to be impossible (due to the ghost issue) even for an increasing number of HT terms. This means that the lower bound of the pQCD applicability (supported by power HT terms) now may be shifted down to  $Q \sim \Lambda_{QCD} \simeq 350$  MeV.

However, it seems to be difficult to get a description in the region  $Q < \Lambda_{QCD}$ . This is not surprising, because the expansion in positive powers of  $Q^2$  and its matching [9] with the HT expansion are relevant here. In this respect, the  $\Lambda_{QCD}$  scale appears as a natural border between ‘‘higher-twist’’ and ‘‘chiral’’ nonperturbative physics.

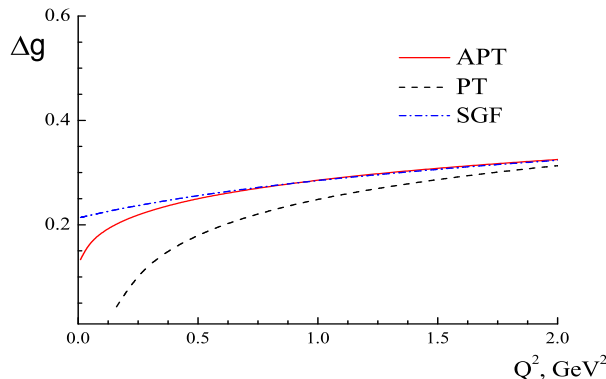


FIG. 10: Scale dependence of the gluon polarization  $\Delta g$ , obtained for different versions of perturbation theory – in APT (solid line), in conventional PT (dashed line), and in the SGF model (dash-dotted line).

Finally, in Fig. 10, we show the scale dependence of the gluon polarization  $\Delta g$  obtained in APT, PT, and the SGF model. In conventional PT the value of  $\Delta g$  is small at the lower

scale  $Q^2 \sim 0.3 \text{ GeV}^2$  (see Ref. [55]). However, as one can see from Fig. 10, one may evolve  $\Delta g$  starting from higher scales  $Q^2 > 1 \text{ GeV}^2$  down to the deep infrared region and observe that the smallness of  $\Delta g$  is a consequence of the Landau singularities in  $\alpha_s$ . Applying different ghost-free models we see that  $\Delta g$  is much higher at  $Q^2 \lesssim 0.5 \text{ GeV}^2$  than one predicted in the standard PT.

## V. CONCLUSION AND OUTLOOK

The singlet axial charge  $a_0$  is the essential element of the nucleon spin structure which is related to the average total quark polarization in the nucleon. In this paper, we systematically extracted this quantity from very accurate JLab data on the first moments of spin structure functions  $g_1^{p,n}$ .

These data were obtained at low  $Q^2$  region  $0.05 < Q^2 < 3 \text{ GeV}^2$ , and therefore, a special attention was paid to the QCD coupling in this domain. We demonstrated that the denominator form (2.10) of the QCD coupling  $\alpha_s$  is more suitable at the low  $Q^2$  (see Figs. 1 and 2). In particular, at the two-loop level it happens to be quite close to the exact numerical solution of the corresponding two-loop RG equation for  $Q \gtrsim 0.5 \text{ GeV}$ .

The performed analysis includes even lower  $Q \sim \Lambda_{QCD}$  and involves the QCD coupling which is free of Landau singularities. For this purpose we used the APT [14] and the soft glueball-freezing model [17] for the infrared-finite QCD coupling  $\alpha_s$ . It was shown that the singularity-free APT and SGF QCD couplings are very close in the domain  $Q \gtrsim 400 \text{ MeV}$ .

One can argue that large order perturbative and nonperturbative contributions are mixed up, and the duality between them is expected (see Ref. [56]). We tested a separation of perturbative and nonperturbative physics and performed a systematic comparison of the extracted values of the higher-twist terms in different versions of perturbation theory. A kind of duality between higher orders of PT and HT terms is observed so that higher order terms absorb part of the HT contributions moving the pQCD frontier between the PT and HT contribution to lower  $Q$  values in both nonsinglet and singlet channels (see Fig. 3). As expected, the value of  $a_0$  changes substantially when coming from LO to NLO, whereas it is quite stable in higher-loop approximations.

The perturbative contribution to the proton spin sum rule  $\Gamma_1^p$  and to the Bjorken sum rule  $\Gamma_1^{p-n}$  in the APT approach and the SGF model is less than 5 % for  $Q > \Lambda$ . This explains the similarity of the extracted higher-twist parameters for these two modifications of QCD couplings.

In the APT approach the convergence of both the higher orders and HT series is much better. In both the nonsinglet and singlet case, while the twist-4 term happened to be larger in magnitude in the APT than in the conventional PT, the subsequent terms are essentially smaller and quickly decreasing (as the APT absorbs some part of nonperturbative dynamics described by HT). This is the main reason for the shift of the pQCD frontier to lower  $Q$  values. A satisfactory description of the proton SSR and BSR data down to  $Q \sim \Lambda_{QCD} \simeq 350 \text{ MeV}$  was achieved by taking the higher-twist and (analytic) higher order perturbative contributions into account simultaneously (see Figs. 6 and 7). The best accuracy for the extracted values of  $a_0$  and higher-twist contributions  $\mu_{2i}$  is achieved for the most precise proton SSR data while the analysis of the data on the neutron SSR shows the compatibility with the analysis of the BSR which is free from the singlet contribution.

For the first time we considered the QCD evolution at low  $Q^2$  of both the leading twist  $a_0$  and the higher-twist  $\mu_4$  terms using the (fractional) analytic perturbation theory [54] and

also the related evolution of the average gluon polarization  $\Delta g$ . Account of this evolution, which is most important at low  $Q^2$ , improves the stability of the extracted parameters whose  $Q^2$  dependence diminishes (see Table VII). As a result, we extract the value of the singlet axial charge  $a_0(1 \text{ GeV}^2) = 0.33 \pm 0.05$ . This value is very close to the corresponding COMPASS  $0.35 \pm 0.06$  [28] and HERMES  $0.35 \pm 0.06$  [29] results.

The RG evolution of  $a_0$  is related to the evolution of the average gluon polarization  $\Delta g$  [1, 2]. The results of the evolution of  $\Delta g$  in the analytic perturbation theory and in the standard PT was compared (see Fig. 10). The decrease of  $\Delta g$  at low  $Q^2$  in APT is not so dramatic as in the standard PT case [55].

In a sense, it could be natural if the main reason for the significant shift of the pQCD frontier to lower  $Q^2$  scales was the disappearance of unphysical singularities in perturbative series. Note that the data at very low  $Q \sim \Lambda_{QCD}$  are usually dropped from the analysis of  $a_0$  and the higher-twist term in the standard PT analysis because of Landau singularities. At the same time, the compatibility of our results for  $a_0$ , extracted from the low energy JLab data with previous results [28, 29] demonstrates the universality of the nucleon spin structure at large and low  $Q^2$  scales. It will be very interesting to explore the interplay between perturbative and nonperturbative physics against other low energy experimental data.

## ACKNOWLEDGMENTS

This work was partially supported by RFBR Grants No. 07-02-91557, No. 08-01-00686, No. 08-02-00896-a, and No 09-02-66732, the JINR-Belorussian Grant (Contract No. F08D-001), and RF Scientific School Grant No. 1027.2008.2. We are thankful to A.P. Bakulev, J.P. Chen, G. Dodge, A.E. Dorokhov, S.B. Gerasimov, G. Ingelman, A.L. Kataev, S.V. Mikhailov, A.V. Sidorov, D.B. Stamenov, and N.G. Stefanis for valuable discussions.

- 
- [1] M. Anselmino, A. Efremov and E. Leader, Phys. Rept. **261**, 1 (1995) [Erratum-ibid. **281**, 399 (1997)].
  - [2] S. E. Kuhn, J. P. Chen and E. Leader, Prog. Part. Nucl. Phys. **63**, 1 (2009).
  - [3] A. V. Efremov, J. Soffer and O. V. Teryaev, Nucl. Phys. **B346**, 97 (1990).
  - [4] O. V. Teryaev, To appear in Proceedings of XIII Workshop of High Energy Spin Physics, DSPIN'09, Dubna, Russia September 1 - 5, 2009.
  - [5] M. V. Polyakov, A. Schafer and O. V. Teryaev, Phys. Rev. D **60**, 051502 (1999) [arXiv:hep-ph/9812393].
  - [6] R. S. Pasechnik, D. V. Shirkov and O. V. Teryaev, Phys. Rev. D **78**, 071902 (2008).
  - [7] J. D. Bjorken, Phys. Rev. **148**, 1467 (1966); Phys. Rev. D **1**, 1376 (1970).
  - [8] J. Kodaira *et al.*, Nucl. Phys. **B159**, 99 (1979);  
J. Kodaira, Nucl. Phys. **B165**, 129 (1980);  
S. A. Larin, F. V. Tkachov and J. A. Vermaseren, Phys. Rev. Lett. **66**, 862 (1991);  
S. A. Larin and J. A. Vermaseren, Phys. Lett. B **259**, 345 (1991);  
M. Anselmino, B. L. Ioffe and E. Leader, Sov. J. Nucl. Phys. **49**, 136 (1989).
  - [9] J. Soffer and O. Teryaev, Phys. Rev. Lett. **70**, 3373 (1993); Phys. Rev. D **70**, 116004 (2004).

- [10] M. Osipenko *et al.*, Phys. Lett. B **609**, 259 (2005) [arXiv:hep-ph/0404195].
- [11] A. Deur, V. Burkert, J. P. Chen and W. Korsch, Phys. Lett. B **665**, 349 (2008).
- [12] D. V. Shirkov, Nucl. Phys. Proc. Suppl. **162**, 33 (2006).
- [13] C. Amsler *et al.* [Particle Data Group], Phys. Lett. B **667**, 1 (2008).
- [14] D. V. Shirkov and I. L. Solovtsov, JINR Rapid Comm. **2** [76-96], 5 (1996) [arXiv:hep-ph/9604363]; Phys. Rev. Lett. **79**, 1209 (1997);  
K. A. Milton and I. L. Solovtsov, Phys. Rev. **D 55**, 5295 (1997).
- [15] D. V. Shirkov and I. L. Solovtsov, Theor. Math. Phys. **150**, 132 (2007).
- [16] M. Baldicchi, A. V. Nesterenko, G. M. Prospero, D. V. Shirkov and C. Simolo, Phys. Rev. Lett. **99**, 242001 (2007).
- [17] Yu. A. Simonov, Phys. Atom. Nucl. **65**, 135 (2002); **66**, 764 (2003); J. Nonlin. Math. Phys. **12**, S625 (2005).
- [18] M. Beneke, Phys. Rept. **317**, 1 (1999).
- [19] G. Curci, M. Greco and Y. Srivastava, Phys. Rev. Lett. **43**, 834 (1979); Nucl. Phys. **B159**, 451 (1979);  
C. Berger *et al.* [PLUTO Collaboration], Phys. Lett. B **100**, 351 (1981);  
J. M. Cornwall, Phys. Rev. D **26**, 1453 (1982);  
N. G. Stefanis, Phys. Rev. D **40**, 2305 (1989) [Erratum-ibid. D **44**, 1616 (1991)];  
N. N. Nikolaev and B. M. Zakharov, Z. Phys. C **49**, 607 (1991); C **53**, 331 (1992);  
Y. L. Dokshitzer, V. A. Khoze and S. I. Troian, Phys. Rev. D **53**, 89 (1996).
- [20] K. V. Dharmawardane *et al.*, Phys. Lett. **B 641** 11 (2006);  
P. E. Bosted *et al.*, Phys. Rev. C **75**, 035203 (2007);  
Y. Prok *et al.* [CLAS Collaboration], Phys. Lett. B **672**, 12 (2009).
- [21] X. D. Ji and J. Osborne, J. Phys. G **27**, 127 (2001).
- [22] S. B. Gerasimov, Yad. Fiz. **2**, 598 (1965) [Sov. J. Nucl.Phys. **2**, 430 (1966)];  
S. D. Drell and A. C. Hearn, Phys. Rev. Lett. **16**, 908 (1966).
- [23] A. L. Kataev, Phys. Rev. D **50**, 5469 (1994); Mod. Phys. Lett. A **20**, 2007 (2005).
- [24] S. A. Larin, T. van Ritbergen and J. A. M. Vermaseren, Phys. Lett. B **404**, 153 (1997).
- [25] Y. Goto *et al.* [Asymmetry Analysis collaboration], Phys. Rev. D **62**, 034017 (2000).
- [26] E. V. Shuryak and A. I. Vainshtein, Nucl. Phys. **B199**, 451 (1982); **B201**, 141 (1982).
- [27] J. P. Chen, nucl-ex/0611024;  
J. P. Chen, A. Deur and Z. E. Meziani, Mod. Phys. Lett. A **20**, 2745 (2005).
- [28] V. Y. Alexakhin *et al.* [COMPASS Collaboration], Phys. Lett. B **647**, 8 (2007).
- [29] A. Airapetian *et al.* [HERMES Collaboration], Phys. Rev. D **75**, 012007 (2007).
- [30] E. Leader, A. V. Sidorov and D. B. Stamenov, Phys. Rev. D **75**, 074027 (2007).
- [31] D. de Florian, R. Sassot, M. Stratmann and W. Vogelsang, Phys. Rev. Lett. **101**, 072001 (2008).
- [32] M. Hirai and S. Kumano [Asymmetry Analysis Collaboration], Nucl. Phys. **B813**, 106 (2009).
- [33] R. Fatemi *et al.* [CLAS Collaboration], Phys. Rev. Lett. **91**, 222002 (2003);  
M. Amarian *et al.*, Phys. Rev. Lett. **89**, 242301 (2002);  
M. Amarian *et al.* [Jefferson Lab E94-010 Collaboration], Phys. Rev. Lett. **92**, 022301 (2004).
- [34] G. Cvetič, A. Y. Illarionov, B. A. Kniehl and A. V. Kotikov, Phys. Lett. B **679**, 350 (2009) [arXiv:0906.1925 [hep-ph]].
- [35] A. Deur *et al.*, Phys. Rev. D **78**, 032001 (2008).
- [36] A. Deur, arXiv:nucl-ex/0508022.
- [37] Z. E. Meziani *et al.*, Phys. Lett. B **613**, 148 (2005) [arXiv:hep-ph/0404066].

- [38] A. Deur *et al.*, Phys. Rev. Lett. **93**, 212001 (2004) [arXiv:hep-ex/0407007].
- [39] S. Bethke, arXiv:0908.1135 [hep-ph].
- [40] K. A. Milton, I. L. Solovtsov and O. P. Solovtsova, Phys. Rev. D **60**, 016001 (1999).
- [41] A. V. Kotikov, G. Parente and J. Sanchez Guillen, Z. Phys. C **58**, 465 (1993).
- [42] G. Parente, A. V. Kotikov and V. G. Krivokhizhin, Phys. Lett. B **333**, 190 (1994) [arXiv:hep-ph/9405290].
- [43] A. L. Kataev, A. V. Kotikov, G. Parente and A. V. Sidorov, Phys. Lett. B **417**, 374 (1998) [arXiv:hep-ph/9706534].
- [44] A. L. Kataev, G. Parente and A. V. Sidorov, Nucl. Phys. **B573**, 405 (2000).
- [45] M. A. Shifman, A. I. Vainshtein and V. I. Zakharov, Nucl. Phys. **B147**, 385 (1979).
- [46] V. D. Burkert and B. L. Ioffe, Phys. Lett. B **296**, 223 (1992).
- [47] W. Wetzel, Nucl. Phys. B **139**, 170 (1978).
- [48] Ashok suri, Phys. Rev. D **4**, 570 (1971).
- [49] K. A. Milton, I. L. Solovtsov and O. P. Solovtsova, Phys. Lett. B **439**, 421 (1998).
- [50] B. A. Magradze, JINR Comm. E2-2000-222, Oct 2000. 19 pp. [hep-ph/0010070].
- [51] D. S. Kourashev and B. A. Magradze, Theor. Math. Phys., **135**, 531 (2003) [hep-ph/0104142].
- [52] I. L. Solovtsov and D. V. Shirkov, Theor. Math. Phys. **120**, 1220 (1999).
- [53] D. V. Shirkov and A. V. Zayakin, Phys. Atom. Nucl. **70**: 775-783, (2007).
- [54] A. P. Bakulev, S. V. Mikhailov and N. G. Stefanis, Phys. Rev. D **72**, 074014 (2005) [Erratum-ibid. D **72**, 119908 (2005)]; **75**, 056005 (2007) [Erratum-ibid. D **77**, 079901 (2008)]; N. G. Stefanis, arXiv:0902.4805 [hep-ph].
- [55] M. Wakamatsu and Y. Nakakoji, Phys. Rev. D **77**, 074011 (2008).
- [56] S. Narison and V. I. Zakharov, Phys. Lett. B **679**, 355 (2009) [arXiv:0906.4312 [hep-ph]].